Journal of ELECTRONIC MATERIALS, Vol. 48, No. 3, 2019
https://doi.org/10.1007/s11664-018-6637-3

The Effect of Core–Shell Structure on Microwave Absorption Properties of Graphite-Coated Magnetic Nanocapsules

YANG FENG,[1] DA LI,[1,4] YU BAI,[1] AN HUA,[1] DESHENG PAN,[1] YONG LI,[1] YU WANG,[2] JUN HE,[2] ZHENHUA WANG,[1] YAJING ZHANG,[3] WEI LIU,[1] and ZHIDONG ZHANG[1]

1.—Shenyang National Laboratory for Materials Science, Institute of Metal Research, Chinese Academy of Sciences, Shenyang 110016, China. 2.—Division of Functional Materials, Central Iron and Steel Research Institute, Beijing 100081, China. 3.—College of Chemical Engineering, Shenyang University of Chemical Technology, Shenyang 110142, China. 4.—e-mail: dali@imr.ac.cn

Interface polarization is one important factor in producing a good electromagnetic impedance match and enhancing the microwave-absorption properties of core/shell nanocomposites. However, the effect of the core–shell nanocapsules having insulating shells, and the polarization effect at interfaces of graphite-coated magnetic metallic nanoparticles, on the microwave absorption properties, are not clear. In this work, the microwave-absorption properties of magnetic nanocapsules with α-Fe/γ-Fe(C)/Fe_3C as cores and graphite as shells have been investigated in the frequency range 2–18 GHz. Partial magnetic cores were removed by a $\sim$ 19 wt.% HCl solution from the as-prepared nanocapsules (A-nanocapsules), but the carbon shells were kept constant. Transmission electron microscopy confirms that hollow carbon nanocages are almost the same as the as-prepared shells, except for slight change in shape due to removing the cores. As a result, the complex permeability drops slightly, while the complex permittivity has an obvious increase, which can be ascribed to percolation effects due to the hollow carbon nanocages, rather than the interface polarization originating from the core/shell interfaces and interfaces between the core components of α-Fe, γ-Fe(C) and Fe_3C nanocrystals. The optimal reflection loss (RL) value of the A-nanocapsules reaches $-$ 27.6 dB at 16.2 GHz for a thickness of 2 mm. This study clarifies that the interface polarization effect in the A-nanocapsules is negligible in enhancing the complex permittivity and the synergetic effect of the magnetic loss of cores, and the dielectric loss of graphite shells is the dominant mechanism in attenuating microwaves.

Key words: Microwave absorption mechanism, impedance matching, interface effect, core/shell structure

INTRODUCTION

With the explosive development of electronic and electrical industrial activities in the gigahertz-frequency range, electromagnetic (EM) pollution has become a serious problem for society.[1–3] To settle this invisible and omnipresent problem, many efforts have been devoted to exploring a variety of microwave absorption materials for stealth or shielding. Microwave absorption performance is determined by the complex permeability/permittivity, the EM impedance matching and the microstructure of the absorbents. Among the EM wave absorbents, magnetic/dielectric nanocomposites with a core/shell structure have attracted worldwide interest due to their interface

(Received June 30, 2018; accepted August 30, 2018; published online September 11, 2018)

polarization and the synergetic effect of their magnetic and dielectric losses.[4–7] In comparison with a mixture of iron and carbon,[8] shell-coated metallic magnetic nanocapsules, such as Fe/C,[9,10] present an enhanced reflection loss (RL) (exceeding − 20 dB) in the frequency range 3.2–18 GHz. An optimal RL value of − 43.5 dB was reached at 9.6 GHz for an absorber thickness of 3.1 mm. In the case of FeCo/C nanocapsules, the broadest bandwidth (RL values exceeding − 10 dB) covers from 10 to 18 GHz, half of the X-band and the whole Ku-band at the 2 mm layer thickness.[11] Fe/SiO_2[12] with a varied shell constituent exhibits multi-loss mechanisms for EM wave absorption. An increase of the disorder in carbon shells results in a redshift of the reflection loss peak to a lower frequency, in which different charge transfers at the core/shell interface were found in $Fe_{55}Co_{45}$/(C, silicides)[13] and Ni/(C, silicides) nanocapsules.[6] Moreover, various cores and shells, such as Fe(Mn)/ferrite nanocapsules,[5] Ni/C,[14] Co/C nanofiber,[15] CoNi/C[16] and α-Fe(N)[17] also exhibit optimized microwave absorption performance. Core double–shell nanocomposites including FeCo/C/$BaTiO_3$,[7] FeCo/C/(FeCo,$CoFe_2O_4$)[18] and FeCo/C/$Fe_{2.5}Cr_{0.5}Se_4$,[19] were developed to improve the EM impedance matching by interface polarization, thus enhancing their microwave absorption properties.

Compared with insulating ferrite[5] and oxide[12,17,20,21] as dielectric shells, it is not clear that the electrical characteristics of different interfaces in the carbon nanostructures[6,9,11,13,14,16,22] can produce distinct interface effects, and thus influence the microwave-absorption properties of core/shell nanocapsules. In this work, the microwave-absorption properties of magnetic core/shell nanocapsules, with decreasing amounts of magnetic cores, but keeping graphite shells almost constant, have been investigated in the frequency range 2–18 GHz. Reducing the amount of cores and interfaces of graphite-coated magnetic nanocapsules causes an obvious increase in the complex permittivity and dielectric loss, but a significant decrease in the microwave-absorption performance. Our experimental results reveal that the percolation effect, but not interface polarization effect, in the metallic core/shell nanocapsules is responsible for the increase of the complex permittivity and dielectric loss. The synergetic effect between magnetic loss of cores and dielectric loss of carbon shells contributes to excellent microwave absorption properties of the as-synthetic nanocapsules.

EXPERIMENTAL DETAILS

Spherical core/shell nanocapsules (denoted as A-nanocapsules) with core diameter in the range of 10–100 nm and graphite shells in a thickness of 3–7 nm were prepared by the arc-discharge method, in which an iron ingot of 99.9% purity was used as the anode and a graphite needle served as the cathode. High-purity argon was introduced into the evacuated chamber to serve as the plasma source and absolute ethanol was the C source. After the arc-discharge process, residual gases were pumped out and a small amount of air was introduced into the chamber, passivating for 24 h. At last, the nanocapsules were collected for further investigation. Two kinds of methods were used to partially remove the magnetic cores from the A-nanocapsules. In the first case, 200 mg of A-nanocapsules were naturally immersed into 20 mL of concentrated hydrochloric acid (19 wt.% HCl). After sealed and ultrasonicated for 30 min, the mixture was put aside at room temperature and ambient pressure for 6 months. The naturally immersed nanocapsules (N-nanocapsules) were deposited by centrifugation and washed three times with an ethanol/deionized water mixture and dried in a drying oven at 48°C for 1 day. In another case, 200 mg of A-nanocapsules and 20 mL of concentrated hydrochloric acid (19 wt.% HCl) were mixed together and sealed into a 50 mL Teflon-lined autoclave, which was heated to 200°C for 100 h. After cooling down to room temperature, the samples were separated by centrifugation from the mixed solution and were washed several times with absolute ethanol and deionized water. The hydrothermally treated nanocapsules were dried in an oven at 48°C for one day, which were marked as hydrothermally treated nanocapsules (H-nanocapsules).

X-ray diffraction (XRD) patterns of the nanocapsules were recorded with a Rigaku D/Max-2400 diffractometer with Cu-K_α radiation (λ = 0.154056 nm) in the 2θ range of 10°–85° with a step size of 0.02°. Morphology and microstructure of the nanocapsules were observed by scanning electron microscopy (SEM, INSPECT F50) and transmission electron microscopy (TEM, FEI Tednai G2 F20) with an emission voltage of 200 kV. Surface information of the samples was analyzed by x-ray photoelectron spectroscopy (XPS), with an Al-K_α line x-ray source. The degree of disorder of the graphite shells was investigated by Raman spectroscopy (RENISHAW, inVia Raman Microscope). Hysteresis loops of the nanocapsules at 5 and 300 K were measured by a superconducting quantum interference device (SQUID, MPMS XL7, Quantum Design) in the magnetic-field range from − 20 to 20 kOe, while M–T curves were measured in the temperature range of 5-300 K. The complex permittivity ($\varepsilon_r = \varepsilon' - i\varepsilon''$) and complex permeability ($\mu_r = \mu' - i\mu''$) were recorded in the frequency (f) range from 2 to 18 GHz by using an Agilent N5230C vector network analyzer (VNA), where the samples with a weight ratio of 50 wt.% microwave absorbents in the paraffin composites were prepared according to a method described elsewhere.[5] The ε_r and the μ_r were derived from the S-parameters obtained with the calibrated VNA, using a simulation program for the Refection/Transmission Mu and Epsilon (Nicholson–Ross–Weir model).[7]

RESULTS AND DISCUSSION

The XRD patterns in Fig. 1a and b indicate that the composites in the A- and the N-nanocapsules can be indexed with α-Fe (06-0696), γ-Fe(C) (52-0512) and Fe_3C (35-0772) according to the Joint Committee on Powder Diffraction Standards (JCPDS) XRD cards, while the H-nanocapsules are composed of α-Fe (06-0696) and Fe_3C (35-0772). Both α-Fe and Fe_3C are observed in the N- and H-nanocapsules (Fig. 1b and c), even after experiencing a long immersion or solvothermal etching at high temperature and pressure by concentrated HCl acid, while γ-Fe(C) disappears in the H-nanocapsules (Fig. 1c), possibly due to the phase transformation from fcc γ-Fe(C) to bcc α-Fe during the hydrothermal treatment. No characteristic C reflection peaks can be found in Fig. 1a–c because of the thin carbon shell coating on the surface of the cores. High-resolution TEM image of the A-nanocapsules in Fig. 1d shows that the composite α-Fe/γ-Fe(C)/Fe_3C cores are well encapsulated by graphite-type shells. The core diameters are in the range of 10–100 nm and the graphite shell thickness is about 3–7 nm. After naturally HCl etching for 6 months, cores with evidently reduced size and/or hollow carbon nanocages can be observed in the N-nanocapsules (Fig. 1e). The high-resolution TEM image for the H-nanocapsules (Fig. 1f) shows that some cores have been removed completely, and hollow carbon nanocages have emerged. Obviously, the etching by the solvothermal treatment is more complete than immersion at ambient temperature and pressure. Compared with the carbon shells in the A-nanocapsules, the extracted carbon shells slightly deform due to the lack of filling in the cores. However, most of core/shell nanocapsules survived, even after HCl high-temperature etching, remaining entire without any damage. This means that a large amount of carbon coating nanocapsules have perfect shell-coating structure, while a small amount of nanocapsules with imperfect carbon shells tend to be etched by the HCl. Both the core/shell interfaces and the interfaces between nanocrystals of α-Fe, fcc γ-Fe(C) and Fe_3C in the nanocapsules with imperfect carbon shells would be destroyed by HCl etching, which may significantly affect their microwave absorption properties.

Raman spectra in Fig. 1g–i show negligible difference of the D band (1350 cm^{-1}), the G band (1580 cm^{-1}) and the 2D band (2700 cm^{-1}) in the A-, N- and H-nanocapsules, respectively, where the dots represent the experimental data and the solid lines are the Lorentzian fitting. As is well known, Raman spectroscopy is a powerful tool for characterizing sp^2- and sp^3-hybridized carbon atoms and the degree of carbon disorder.[23] The G mode of graphite around 1580 cm^{-1} corresponds to the only first order-resonance with E_{2g} symmetry, which involves the in-plane bond-stretching motion of pairs of C sp^2 atoms,[24] while the D peak around 1350 cm^{-1} is a breathing mode with A_{1g} symmetry involving phonons near the K-zone boundary. This mode is forbidden in perfect graphite and becomes active only in the presence of disorder.[25] The symmetric peaks of the 2D mode around 2700 cm^{-1} indicate 1–5 layers of AB-stacked graphene or multilayer turbostratic graphene.[26,27] Combining the results of the TEM images, one concludes that the graphite shells have 5–10 layers of turbostratic graphene features in the A-, N- and H-nanocapsules. Ferrari et al. reported that the 2D band in graphite with asymmetric features arises from different phonon-assisted inter-valley transitions.[26,28] The ratio of $I(D)/I(G)$ is used to evaluate the degree of disorder of carbon.[29] In our present case, the $I(D)/I(G)$ values calculated for the A-, the N- and the H-nanocapsules are 0.8, 0.9 and 0.8, respectively. Therefore, the degree of disorder of the graphite shells in the N- and the H-nanocapsules is similar to that of A-nanocapsules, suggestive no change of carbon shells under HCl etching at room temperature or 200°C. Surface composition of these three types of nanocapsules was also investigated by XPS (results not shown). The binding energy of C1*s* at about 283.4 indicates the C–Fe bond in Fe_3C. The binding energies at 284.6 and 285.7 eV reveal ordered and disordered carbon in the carbon shells, while those at 288.5 eV indicate carbon composition related to the absorbed products with the C=O bond coming from the oxidation reaction of ethanol during the arc-discharge process. For the Fe2*p* peaks, Fe2$p_{3/2}$ peak at 706.7 eV and Fe2$p_{1/2}$ peak at 719.6 eV belong to α-Fe, while Fe2$p_{3/2}$ peak at 708.1 eV and Fe2$p_{1/2}$ peak at 721.2 eV correspond to Fe_3C. No iron oxides can be detected in these nanocapsules. The area ratios between the ordered and disordered carbon of the N- and the H-nanocapsules are similar to the A-nanocapsules, revealing the same degree of disorder of the carbon shells in accordance with the Raman results.

Hysteresis loops at room temperature in Fig. 2a show that the saturation magnetization values of the A-, the N- and the H-nanocapsules are 109, 85 and 76 emu/g, respectively. The saturation magnetizations of the N- and H-nanocapsules obviously decrease due to partly removing magnetic cores from the nanocapsules. Hollow carbon nanocages were present in the N-nanocapsules and H-nanocapsules, as observed from Fig. 1e and f. The temperature dependence of magnetization for the A-, the N- and the H-nanocapsules, measured in zero-field-cooled (ZFC) and field-cooled (FC) processes under a magnetic field of 200 Oe, is plotted in Fig. 2b. The ZFC magnetizations increase with increasing temperature. Turning points can be seen in the ZFC magnetization curves at about 30 K, which are contributed mainly by some superparamagnetic α-Fe or Fe_3C nanoparticles with their blocking temperatures (T_B) falling in this temperature range. In the temperature range of 30–300 K, a gradual increase of the ZFC magnetization can mainly be ascribed to domain-wall depinning in the

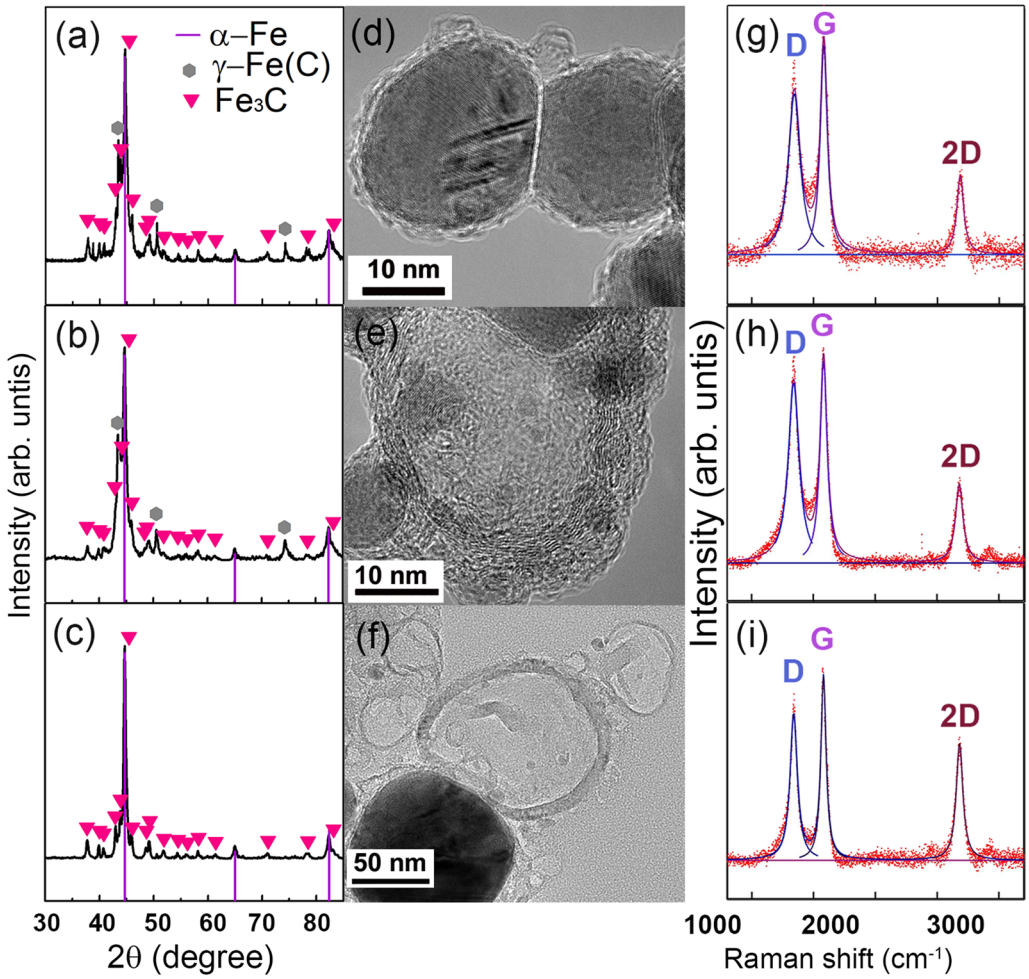

Fig. 1. XRD patterns, TEM images and Raman spectra of (a, d, g) the A-nanocapsules, (b, e, h) the N-nanocapsules and (c, f, i) the H-nanocapsules. The dots in (g, h, i) represent the experimental data and the solid lines correspond to the fitting data.

multi-domain particles, although there remains a contribution of some single-domain particles with blocking temperature in this temperature range.[30] The FC magnetization curves of these three samples all show a simple "Brillouin-like" ferromagnetic behavior.

The real parts of ε' and μ' are associated with the stored electrical and magnetic energy within the absorber and the imaginary parts of ε'' and μ'' associated with the dissipation (or loss) of electrical and magnetic energy. Frequency dependencies of the relative complex permittivity ε_r and the complex permeability μ_r for the A-, the N- and the H-nanocapsules were recorded in the 2–18 GHz frequency range (Fig. 3). Figure 3a and b shows that the ε' and ε'' values increase as the amount of cores in the whole frequency range decreases, whereas the μ' and μ'' values in Fig. 3d and e have a decreasing trend due to reducing the amount of the magnetic cores. The negative imaginary parts (μ'') of the complex permeability within the high frequency microwave range can be ascribed to the measurement errors. Figure 3c and f show the dielectric loss factor ($\tan\delta_\varepsilon = \varepsilon''/\varepsilon'$) and the magnetic loss factor ($\tan\delta_\mu = \mu''/\mu'$) in the frequency range 2–18 GHz. The enhanced dielectric loss factor is observed in the H-nanocapsules, which have more hollow carbon nanocages than the A- and the N-nanocapsules due to removing cores from the carbon nanocages or nanocapsules. The enhancement of ε_r and $\tan\delta_\varepsilon$ in the N- and the H-nanocapsules should not be related to the interface polarization. Usually, we understand that the interface polarization between core and shell in the core/shell nanostructures produces an enhanced relative complex permittivity ε_r, just like the previous report in the core double-shell FeCo/C/$BaTiO_3$.[7] However, in the present case, the number of interfaces between cores and shells and between α-Fe, γ-Fe(C) and Fe_3C nanocrystals in the A-nanocapsules is much larger than that between the N-nanocapsules and H-nanocapsules; but the A-nanocapsules have the lowest ε' and ε''. According to the free electron theory,[31] the imaginary part of the relative complex permittivity of a dielectric material can be evaluated by using the equation: $\varepsilon'' \approx \sigma/(2\pi f\varepsilon_0)$, where σ

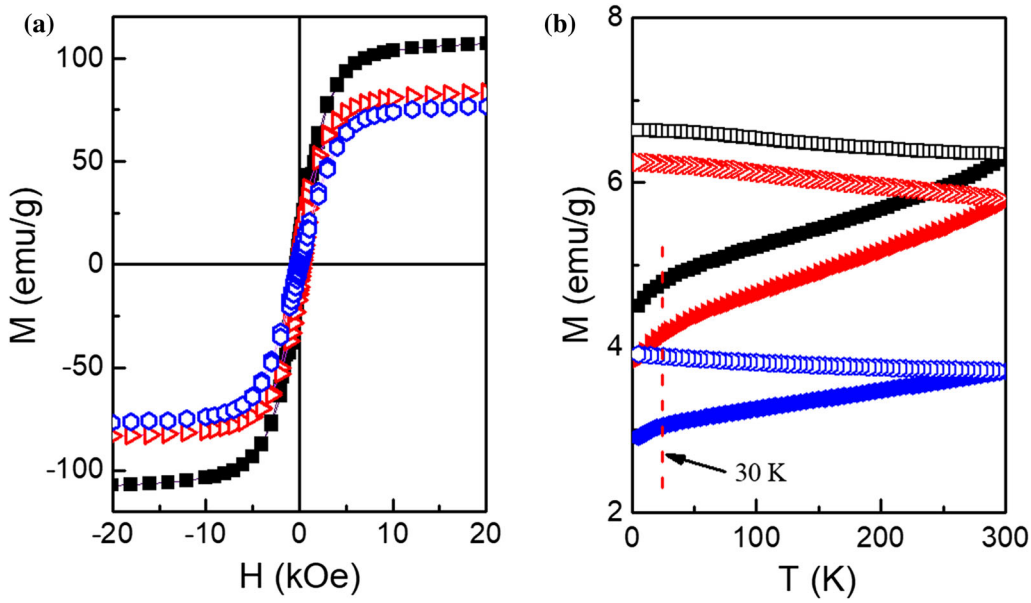

Fig. 2. (a) Room-temperature hysteresis loops and (b) FC (blank dots) and ZFC (solid dots) magnetization curves of the A- (square), the N- (triangle) and the H-nanocapsules (hexagon) recorded in a magnetic field of 200 Oe.

is the electric conductivity (S m^{-1}), ε_0 the free space permittivity (8.854×10^{12} F m^{-1}), f the frequency (Hz). The conductivities of A-, N- and H-nanocapsules-paraffin composites are 4.6×10^{-4}, 3.7×10^{-3} and 0.2 S m^{-1}, respectively. There is a sharp increase of conductivity in 3 orders of magnitude from 4.6×10^{-4} S m^{-1} for the A-nanocapsules-paraffin composite to 2×10^{-1} S m^{-1} for the H-nanocapsules-paraffin composite. Such a change in the conductivity of H-nanocapsules-paraffin composite may be attributed to the percolation effect,[32,33] which is related to the hollow carbon nanocages, rather than to interface polarization. For the 50 wt.% nanocapsules-paraffin composites, there are more nanoparticles in the N- and the H-nanocapsules due to the existence of lighter hollow carbon nanocages. More nanoparticles are helpful in forming the conductive path, when the content of the nanoparticles reaches the threshold percolation. The dielectric resonance phenomena is usually created from space charge polarization, dipole polarization, ionic polarization and electronic polarization. For the metal-based composites, the space charge polarization and the dipole polarization in dielectrics contributes to the absorption of EM energy, which influences the shape of the permittivity as a function of frequency. The fluctuations for ε' and ε'' spectra may be ascribed to the displacement current lag[34] and to the AC loss.[35]

Reflection loss (RL) values can be calculated from the measured complex permittivity (ε_r) and complex permeability (μ_r) at given frequencies and absorber thicknesses by means of the following equations[7]:

$$Z_{\text{in}} = Z_0(\mu_r/\varepsilon_r)^{1/2}\tan h\left[j(2\pi fd/c)(\mu_r\varepsilon_r)^{1/2}\right], \qquad (1)$$

$$\text{RL} = 20\log|(Z_{\text{in}} - Z_0)/(Z_{\text{in}} + Z_0)|, \qquad (2)$$

where Z_{in} is the input impedance of the absorber, Z_0 the characteristic impedance of free space, f the frequency of the EM wave, d the thickness of absorber, c the velocity of light, respectively. Figure 4 presents the frequency dependence of RL for the A-nanocapsules-, the N-nanocapsules- and the H-nanocapsules-paraffin composites. The RL value of − 10 dB corresponds to the microwave-absorption ability of the composites reaching 90%. The A-nanocapsules exhibit a broad absorption bandwidth with RL values exceeding − 10 dB, which covers the 2.3–18 GHz frequency range if an appropriate absorber thickness is chosen, and have an optimal RL value of − 27.6 dB at 16.2 GHz at a thickness of 2 mm (Fig. 4a and d). After HCl etching to remove parts of the magnetic cores, the N-nanocapsules present a minimum RL value of − 8.8 dB at 14.2 GHz at a thickness of 1.5 mm (Fig. 4b and e). However, when more parts of magnetic cores were removed from the nanocapsules, the RL values of the H-nanocapsules do not exceed − 2.3 dB for all thicknesses in the whole measurement frequency range (Fig. 4c and f). The fitting results calculated from the assumed ε_r and μ_r parameters, where all the positive values in the $\varepsilon_r - f$ and $\mu_r - f$ (Fig. 3) were kept, but negative μ'' values were replaced by zero, are very similar to those presented in Fig. 4c and f, indicating that the influence of the measurement errors of μ'' on the microwave absorption properties of H-nanocapsules is tiny and can be neglected. Degree of degradation of the microwave-absorption ability should connect with the varied microstructure and the decrease of magnetic cores

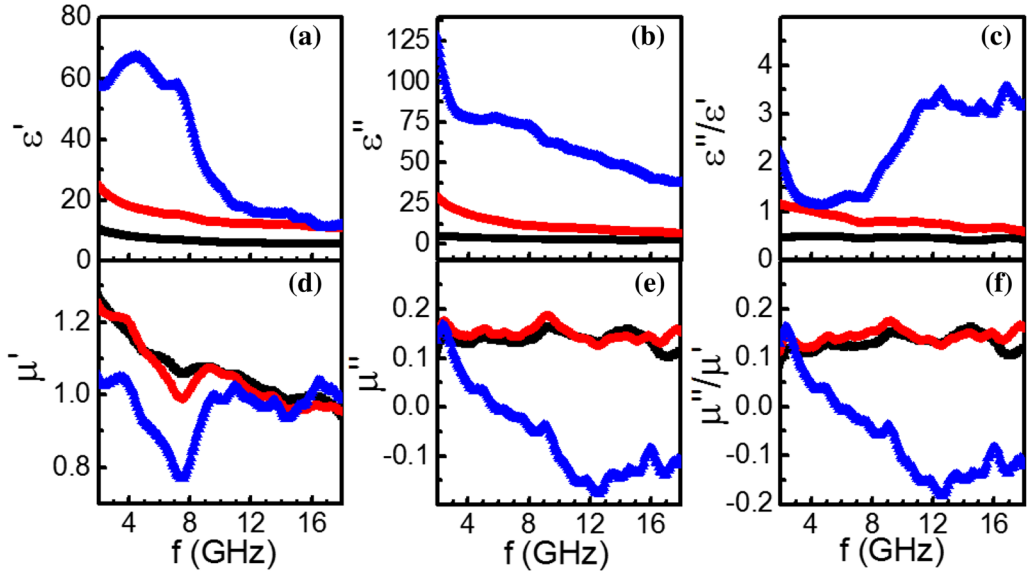

Fig. 3. Frequency dependence of (a) ε', (b) ε'', (c) dielectric loss factor ($\varepsilon''/\varepsilon'$), (d) μ', (e) μ'' and (*f*) magnetic loss factor (μ''/μ') of the A- (black square), the N- (red circle) and the H-nanocapsules (blue triangle) (Color figure online).

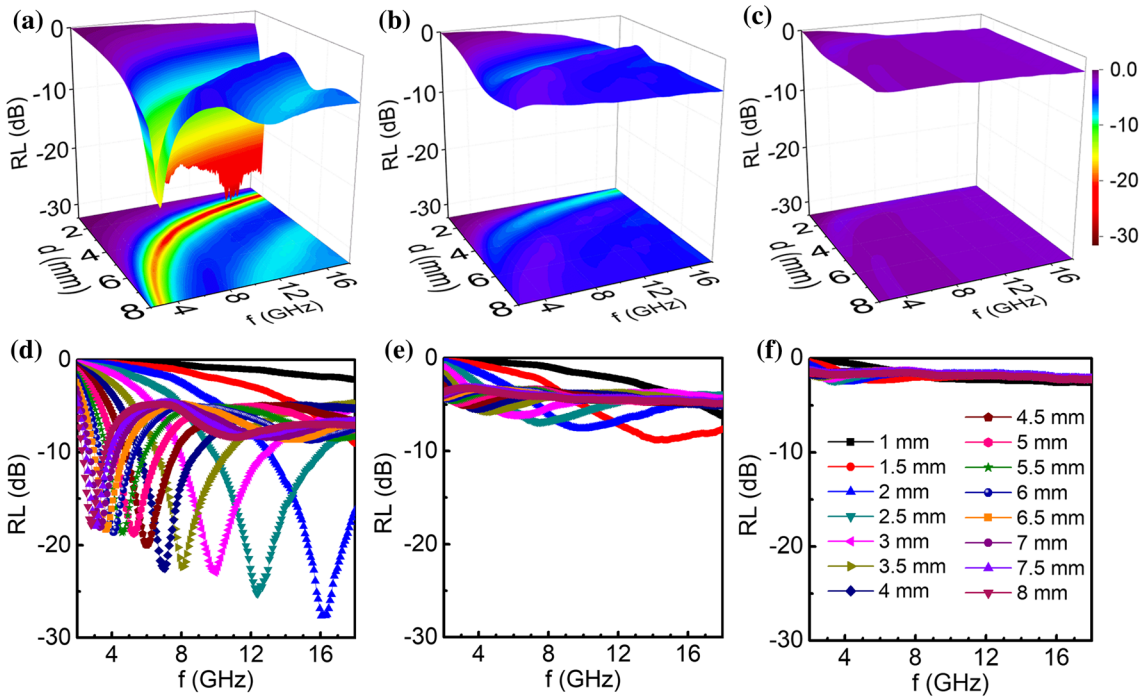

Fig. 4. Frequency dependence of three-dimensional and two-dimensional RLs of (a, d) the A-nanocapsules-paraffin composite, (b, e) the N-nanocapsules-paraffin composite and (c, f) the H-nanocapsules-paraffin composite.

in both the N-nanocapsules and the H-nanocapsules. On one hand, parts of magnetic cores were removed from the core–shell nanostructures to form hollow carbon nanocages, which destroys the synergistic effect of the magnetic and dielectric losses of the cores and shells. On the other hand, to keep the mass ratio of 50 wt.% between the nanocapsules and paraffin, the number of H-nanocapsules exceeds that of the A nanocapsules, which results in an increase of σ and thus larger values of ε_r and $\tan\delta_\varepsilon$. Although the ε_r and $\tan\delta_\varepsilon$ have obvious increases in the N-nanocapsules- and the H-nanocapsules-paraffin composites, the EM wave absorption of the N- and the H-nanocapsules-paraffin composites becomes worse due to bad EM impedance matching. The reduction of microwave absorption properties of the N- and the H-nanocapsules may be ascribed to their poor EM impedance matching, whereas the

good microwave absorption properties of the A-nanocapsules result from an excellent synergistic effect of the magnetic and dielectric losses of the cores and shells.

CONCLUSIONS

Graphite-coated magnetic α-Fe/γ-Fe(C)/Fe_3C nanocapsules with multi-interface structures were prepared by the arc-discharge method. The microwave-absorption properties of the nanocapsules have been investigated in the frequency range 2–18 GHz, while reducing the amount of magnetic cores but keeping graphite shells constant. In comparison with the A-nanocapsules, part of the magnetic cores were removed to obtain the N- and H-nanocapsules. TEM images confirm that hollow graphite nanocages are almost the same as the shells in the A-nanocapsules, except for a slight change in shape after removing the cores. The complex permeability drops slightly with reduction of the magnetic cores, while the complex permittivity has an obvious increase. Although there are a large number of interfaces between the cores and the shells and between the core components of α-Fe, γ-Fe(C) and Fe_3C nanocrystals, the interface polarization behavior may make a slight contribution to the dielectric loss due to good conduction of metallic cores and graphite shells. The optimal reflection loss (RL) value of the A-nanocapsules reaches − 27.6 dB at 16.2 GHz for a thickness of 2 mm with a broad absorption bandwidth of 15.7 GHz (RL values exceeding − 10 dB), covering the 2.3–18 GHz frequency range by choosing an appropriate absorber thickness. The good microwave absorption performance of the as-prepared core/shell nanocapsules was attributed to the excellent synergistic effect of the magnetic and dielectric losses.

ACKNOWLEDGEMENTS

The work has been supported by the National Natural Science Foundation of China under Grant Nos. 51171185, 51331006, 51371055, 51301114, and the National Basic Research Program (Nos. 2012CB933103 and 2017YFA0206302) of China, Ministry of Science and Technology of China.

REFERENCES

1. B. Sirav and N. Seyhan, *Electromagn. Biol. Med.* 215, 28 (2009).
2. M. Parazzini, S. Bell, G. Thuroczy, F. Molnar, G. Tognola, M.E. Lutman, and P. Ravazzani, *Hear. Res.* 68, 208 (2005).
3. A. Balmori, *Toxicol. Environ. Chem.* 287, 88 (2006).
4. L.W. Jiang, Z.H. Wang, D. Li, D.Y. Geng, Y. Wang, J. An, J. He, W. Liu, and Z.D. Zhang, *RSC Adv.* 40384, 5 (2015).
5. Z. Han, D. Li, X.G. Liu, D.Y. Geng, J. Li, and Z.D. Zhang, *J. Phys. D Appl. Phys.* 055008, 42 (2009).
6. J.J. Jiang, H. Wang, H.H. Guo, T. Yang, W.S. Tang, D. Li, S. Ma, D.Y. Geng, W. Liu, and Z.D. Zhang, *Nanoscale Res. Lett.* 1, 7 (2012).
7. J.J. Jiang, D. Li, D.Y. Geng, J. An, J. He, W. Liu, and Z.D. Zhang, *Nanoscale* 3967, 6 (2014).
8. D. Min, W. Zhou, Y. Qing, F. Luo, and D. Zhu, *J. Electron. Mater.* 4903, 46 (2017).
9. X.F. Zhang, X.L. Dong, H. Huang, B. Lv, J.P. Lei, and C.J. Choi, *J. Phys. D Appl. Phys.* 5383, 40 (2007).
10. X. Zhao, Z. Zhang, L. Wang, K. Xi, Q. Cao, D. Wang, Y. Yang, and Y. Du, *Sci. Rep.* 3421, 3 (2013).
11. Z. Han, D. Li, H. Wang, X.G. Liu, J. Li, D.Y. Geng, and Z.D. Zhang, *Appl. Phys. Lett.* 023114, 95 (2009).
12. X.F. Zhang, X.L. Dong, H. Huang, B. Lv, X.G. Zhu, J.P. Lei, S. Ma, W. Liu, and Z.D. Zhang, *Mater. Sci. Eng., A* 211, 454 (2007).
13. J.J. Jiang, X.J. Li, Z. Han, D. Li, Z.H. Wang, D.Y. Geng, S. Ma, W. Liu, and Z.D. Zhang, *J. Appl. Phys.* 17A514, 115 (2014).
14. H. Wang, H.H. Guo, Y.Y. Dai, D.Y. Geng, Z. Han, D. Li, T. Yang, S. Ma, W. Liu, and Z.D. Zhang, *Appl. Phys. Lett.* 083116, 101 (2012).
15. J. Zhang, P. Wang, Y. Chen, G. Wang, D. Wang, L. Qiao, T. Wang, and F. Li, *J. Electron. Mater.* 4703, 47 (2018).
16. H. Wang, Y.Y. Dai, W.J. Gong, D.Y. Geng, S. Ma, D. Li, W. Liu, and Z.D. Zhang, *Appl. Phys. Lett.* 223113, 102 (2013).
17. D. Li, C.J. Choi, Z. Han, X.G. Liu, W.J. Hu, J. Li, and Z.D. Zhang, *J. Magn. Magn. Mater.* 4081, 321 (2009).
18. Y. Feng, D. Li, L.W. Jiang, Z.M. Dai, Y. Wang, J. An, W.J. Ren, J. He, Z.H. Wang, W. Liu, and Z.D. Zhang, *J. Alloys Compd.* 1224, 694 (2017).
19. D. Li, Y. Feng, D.S. Pan, L.W. Jiang, Z.M. Dai, S.J. Li, Y. Wang, J. He, W. Liu, and Z.D. Zhang, *RSC Adv.* 73020, 6 (2016).
20. X.G. Liu, D.Y. Geng, and Z.D. Zhang, *Appl. Phys. Lett.* 243110, 92 (2008).
21. X.G. Liu, D.Y. Geng, H. Meng, P.J. Shang, and Z.D. Zhang, *Appl. Phys. Lett.* 173117, 92 (2008).
22. L.W. Jiang, Z.H. Wang, D.Y. Geng, Y.M. Lin, Y. Wang, J. An, J. He, D. Li, W. Liu, and Z.D. Zhang, *Carbon* 910, 95 (2015).
23. D. Li, Z. Han, B. Wu, D.Y. Geng, and Z.D. Zhang, *J. Phys. D Appl. Phys.* 115005, 41 (2008).
24. D.S. Knight and W.B. White, *J. Mater. Res.* 385, 4 (1989).
25. Y. Hernandez, V. Nicolosi, M. Lotya, F.M. Blighe, Z. Sun, S. De, I.T. McGovern, B. Holland, M. Byrne, Y.K. Gun'Ko, J.J. Boland, P. Niraj, G. Duesberg, S. Krishnamurthy, R. Goodhue, J. Hutchison, V. Scardaci, A.C. Ferrari, and J.N. Coleman, *Nat. Nanotechnol.* 563, 3 (2008).
26. A.C. Ferrari, J.C. Meyer, V. Scardaci, C. Casiraghi, M. Lazzeri, F. Mauri, S. Piscanec, D. Jiang, K.S. Novoselov, S. Roth, and A.K. Geim, *Phys. Rev. Lett.* 187401, 97 (2006).
27. D.R. Lenski and M.S. Fuhrer, *J. Appl. Phys.* 013720, 110 (2011).
28. A.C. Ferrari and J. Robertson, *Phys. Rev. B* 14095, 61 (2000).
29. C.N.R. Rao, A.K. Sood, K.S. Subrahmanyam, and A. Govindaraj, *Angew. Chem. Int. Ed.* 7752, 48 (2009).
30. Z.D. Zhang, J.L. Yu, J.G. Zheng, I. Skorvanek, J. Kovac, X.L. Dong, Z.J. Li, S.R. Jin, H.C. Yang, Z.J. Guo, W. Liu, and X.G. Zhao, *Phys. Rev. B* 024404, 64 (2001).
31. S. Ramo, J.R. Whinnery, and T. Van Duzer, *Fields and Waves in Communication Electronics*, 2nd ed. (New York: Wiley, 1984), p. 181.
32. J.J. Jiang, D. Li, S.J. Li, Z.H. Wang, Y. Wang, J. He, W. Liu, and Z.D. Zhang, *RSC Adv.* 14584, 5 (2015).
33. Z. Han, D. Li, X.W. Wang, and Z.D. Zhang, *J. Appl. Phys.* 109, 07A301 (2011).
34. P.C.P. Watts, D.R. Ponnampalam, W.K. Hsu, A. Barnes, and B. Chambers, *Chem. Phys. Lett.* 378, 609–614 (2003).
35. Y.J. Li, C.Z. Zhu, and C.M. Wang, *J. Phys. D Appl. Phys.* 125303, 41 (2008).